Supporting Information: Efficient and Accurate Prediction of Nuclear Magnetic Resonance Shielding Tensors with Double-Hybrid Density Functional Theory

Georgi L. Stoychev, Alexander A. Auer, and Frank Neese*

Max-Planck-Institut für Kohlenforschung, Mülheim an der Ruhr 45470, Germany

E-mail: frank.neese@kofo.mpg.de

S1 Density Functional Terms

The DFT XC energy contribution is

$$E_{\mathrm{XC}}^{\mathrm{DFT}} = \int f\left[\rho\left(\mathbf{r}\right), \gamma\left(\mathbf{r}\right)\right] \mathrm{d}\mathbf{r} \tag{S1}$$

where we have assumed that f is a GGA functional which depends, in the closed-shell case, on the electronic density ρ and its gradient invariant γ expressed using the SCF density matrix $\mathbf{P}$ as

$$\rho_{\mathbf{P}} = \sum_{\mu\nu} P_{\mu\nu}\varphi_\mu\varphi_\nu = \sum_{\mu\nu} P_{\mu\nu}\Omega_{\mu\nu} \tag{S2}$$

$$\gamma_{\mathbf{P}} = \left|\nabla\rho_{\mathbf{P}}\right|^2 \tag{S3}$$

$$\nabla\rho_{\mathbf{P}} = \sum_{\mu\nu} P_{\mu\nu}\nabla\Omega_{\mu\nu} \tag{S4}$$

where $\Omega_{\mu\nu}$ is the overlap distribution of the AOs φ_μ and φ_ν. The Fock matrix therefore also contains an XC potential term:[S1]

$$F_{\mu\nu} = h_{\mu\nu} + \sum_{\kappa\lambda} P_{\kappa\lambda}\left[\left(\mu\nu\,|\,\kappa\lambda\right) - \frac{c_{\mathrm{X}}}{2}\left(\mu\lambda\,|\,\kappa\nu\right)\right] + V_{\mu\nu}^{\mathrm{XC}} \tag{S5}$$

$$V_{\mu\nu}^{\mathrm{XC}} = \int\left[\frac{\partial f}{\partial\rho}\Omega_{\mu\nu} + 2\frac{\partial f}{\partial\gamma}\nabla\rho_{\mathbf{P}}\nabla\Omega_{\mu\nu}\right]\mathrm{d}\mathbf{r} \tag{S6}$$

Note that the DFT exchange and correlation scaling coefficients – $(1 - c_{\mathrm{X}})$ and c_{C}, respectively – are implicitly included in the definition of f.

$\mathbf{V}^{\mathrm{XC}}$ depends on the MO coefficients through $\mathbf{P}$ and therefore minimizing the MP2 Lagrangian with respect to orbital rotations gives rise to the additional Fock response term $\mathcal{R}^{\mathrm{XC}}$ in eq 16 (in the main text) which is given by

$$\mathcal{R}^{\mathrm{XC}}\left[\mathbf{D}\right]_{pq} = 4\sum_{\mu\nu} c_{\mu p}c_{\nu q}\int\left\{\left[\frac{\partial^2 f}{\partial\rho^2}\left[\mathbf{P}\right] + 2\frac{\partial^2 f}{\partial\rho\partial\gamma}\left[\mathbf{P}\right]\right]\rho_{\mathbf{D}}\Omega_{\mu\nu} + \left[\frac{\partial^2 f}{\partial\gamma\partial\rho}\left[\mathbf{P}\right] + 2\frac{\partial^2 f}{\partial\gamma^2}\left[\mathbf{P}\right]\right]\gamma_{\mathbf{P}}\nabla\rho_{\mathbf{D}}\nabla\Omega_{\mu\nu}\right\}\mathrm{d}\mathbf{r} \tag{S7}$$

where $\rho_{\mathbf{D}} = \sum_{\mu\nu} D_{\mu\nu}\Omega_{\mu\nu}$.

Most common DFs do not have an explicit dependence on the external magnetic field. However, when using GIAOs, the electronic density and its gradient depend on the magnetic field through both $\mathbf{P}$ and the basis functions:

$$P_{\mu\nu}^{\mathbf{B}} = 2\sum_{pi} U_{pi}^{\mathbf{B}}\left(c_{\mu i}c_{\nu p} - c_{\mu p}c_{\nu i}\right) = -P_{\nu\mu}^{\mathbf{B}} \tag{S8}$$

$$\Omega_{\mu\nu}^{\mathbf{B}} = \frac{\mathrm{i}}{2}\left(\mathbf{R}_{MN}\times\mathbf{r}\right)\Omega_{\mu\nu}^{0} = -\Omega_{\nu\mu}^{\mathbf{B}} \tag{S9}$$

$$\left(\nabla\Omega_{\mu\nu}\right)^{\mathbf{B}} = \frac{\mathrm{i}}{2}\left(\mathbf{R}_{MN}\times\mathbf{r}\right)\left(\Omega_{\mu\nu}^{0} + \nabla\Omega_{\mu\nu}^{0}\right) = -\left(\nabla\Omega_{\nu\mu}\right)^{\mathbf{B}} \tag{S10}$$

Where $\mathbf{R}_{MN}$ is the distance vector between the centers of AOs μ and ν. Due to the antisymmetry of the perturbed quantities, the full derivatives of the density and its gradient vanish:

$$\rho_{\mathbf{P}}^{\mathbf{B}} = \sum_{\mu\nu} P_{\mu\nu}^{\mathbf{B}}\Omega_{\mu\nu} + \sum_{\mu\nu} P_{\mu\nu}\Omega_{\mu\nu}^{\mathbf{B}} = 0 \tag{S11}$$

$$\left(\nabla\rho_{\mathbf{P}}\right)^{\mathbf{B}} = \sum_{\mu\nu} P_{\mu\nu}^{\mathbf{B}}\nabla\Omega_{\mu\nu} + \sum_{\mu\nu} P_{\mu\nu}\left(\nabla\Omega_{\mu\nu}\right)^{\mathbf{B}} = 0 \tag{S12}$$

$$\gamma_{\mathbf{P}}^{\mathbf{B}} = 2\nabla\rho_{\mathbf{P}}\left(\nabla\rho_{\mathbf{P}}\right)^{\mathbf{B}} = 0 \tag{S13}$$

Hence, the $\mathcal{R}^{\mathrm{XC}(\mathbf{B})}$ contribution to the first order z-vector equations RHS (eq 20) is

$$\mathcal{R}^{\mathrm{XC}(\mathbf{B})}\left[\mathbf{D}\right]_{pq} = 4\sum_{\mu\nu} c_{\mu p}c_{\nu q}\int\left\{\left[\frac{\partial^2 f}{\partial\rho^2}\left[\mathbf{P}\right] + 2\frac{\partial^2 f}{\partial\rho\partial\gamma}\left[\mathbf{P}\right]\right]\rho_{\mathbf{D}}\Omega_{\mu\nu}^{\mathbf{B}} + \left[\frac{\partial^2 f}{\partial\gamma\partial\rho}\left[\mathbf{P}\right] + 2\frac{\partial^2 f}{\partial\gamma^2}\left[\mathbf{P}\right]\right]\gamma_{\mathbf{P}}\nabla\rho_{\mathbf{D}}\left(\nabla\Omega_{\mu\nu}\right)^{\mathbf{B}}\right\}\mathrm{d}\mathbf{r} \tag{S14}$$

Note that, unlike for geometric perturbations,[S2] terms which include third derivatives of the XC functional vanish.

S2 Perturbed Canonical Orbitals

Due to the last two terms in eq 18, the calculation of the MP2 response density becomes a formally $O\left(N^6\right)$ scaling step. In addition, if the amplitudes are calculated in multiple batches, such that T_{ab}^{ij} are only available for i within the batch, the last term in eq 18 requires amplitudes outside the batch. This was noted by Kollwitz and Gauss in their direct GIAO-MP2 implementation,[S3] who suggested the use of perturbed canonical orbitals,[S4–S6] i.e. choosing

$U_{ij}^{\mathbf{B}}$ coefficients such that the internal block of $\mathbf{F}^{\mathbf{B}}$ vanishes:

$$\begin{aligned} 0 \equiv F_{ij}^{\mathbf{B}} &= U_{ij}^{\mathbf{B}}\varepsilon_i - U_{ji}^{\mathbf{B}}\varepsilon_j + F_{ij}^{(\mathbf{B})} \\ &= U_{ij}^{\mathbf{B}}\varepsilon_i - \left(U_{ij}^{\mathbf{B}} + S_{ij}^{(\mathbf{B})}\right)\varepsilon_j + F_{ij}^{(\mathbf{B})} \end{aligned} \tag{S15}$$

$$U_{ij}^{\mathbf{B}} = \frac{F_{ij}^{(\mathbf{B})} - S_{ij}^{(\mathbf{B})}\varepsilon_j}{\varepsilon_j - \varepsilon_i} \tag{S16}$$

Thus the internal Fock matrix contribution to $\mathbf{T}^{ij,\mathbf{B}}$ vanishes and the formal scaling is reduced to $O\left(N^5\right)$. A complication arises when (near-)degenerate orbitals i and j are present which would make the denominator of eq S16 (near-)zero. In these cases $U_{ij}^{\mathbf{B}}$ are chosen according to eq 29 and the corresponding contributions to the perturbed amplitudes are calculated. Hence, only those amplitudes $\mathbf{T}^{kj}$ ($\mathbf{T}^{ik}$) are required for which $\varepsilon_k \approx \varepsilon_i$ ($\varepsilon_k \approx \varepsilon_j$). In our implementation these amplitudes are either precalculated and stored on disk or reevaluated on the fly. The latter option leads to significant computational overhead and should only be used in the unlikely case (for feasible system sizes) of insufficient disk space.

S3 Frozen Core Terms

Use of the frozen core approximation introduces minor additional complications to MP2 (and therefore DHDFT) second derivatives.[S5] The extra terms are derived for RI-MP2 in the context of geometric and magnetic perturbations in refs S7 and S8, respectively. They are given here for consistency with our notation. An additional constraint enters the Lagrangian, which ensures the block-diagonality of the Fock matrix:

$$\begin{aligned} \mathcal{L} = &\sum_{\bar{i}\geq\bar{j}}\left[\left\langle \mathbf{Y}^{\bar{j}}\mathbf{Y}^{\bar{i},\mathrm{T}}\widetilde{\mathbf{T}}^{\bar{i}\bar{j}}\right\rangle + \left\langle \mathbf{Y}^{\bar{j}*}\mathbf{Y}^{\bar{i}\dagger}\widetilde{\mathbf{T}}^{\bar{i}\bar{j}*}\right\rangle\right] \\ &+ \left\langle \mathbf{D}''\mathbf{F}^{\mathrm{T}}\right\rangle + \sum_{ai} z_{ai}F_{ai} + \sum_{\bar{i}\underline{k}} \check{z}_{\bar{i}\underline{k}}F_{\bar{i}\underline{k}} \end{aligned} \tag{S17}$$

where valence and core orbitals are denoted by an over- and underline respectively. The matrix $\mathbf{D}''$ is only non-zero in the valence and virtual blocks:

$$D''_{\bar{i}\bar{j}} = -\sum_{\bar{k}}\left(1+\delta_{\bar{j}\bar{k}}\right)\left\langle \widetilde{\mathbf{T}}^{\bar{k}\bar{j}*}\mathbf{T}^{\bar{i}\bar{k}}\right\rangle \tag{S18}$$

$$D''_{ab} = \sum_{\bar{i}\geq\bar{j}}\left(\widetilde{\mathbf{T}}^{\bar{j}\bar{i}*}\mathbf{T}^{\bar{i}\bar{j}} + \widetilde{\mathbf{T}}^{\bar{i}\bar{j}*}\mathbf{T}^{\bar{j}\bar{i}}\right)_{ab} \tag{S19}$$

Minimizing $\mathcal{L}$ with respect to rotations between valence and core orbitals gives a closed-form expression for the coefficients $\check{z}$:

$$\check{z}_{\bar{i}\underline{k}} = \frac{2\sum_{aP}\Gamma_{\bar{i}a}^{P}B_{\underline{k}a}^{P}}{\varepsilon_{\bar{i}} - \varepsilon_{\underline{k}}} \tag{S20}$$

The RHSs for the z-vector equations are also different for the virtual-valence and virtual-core blocks:

$$X_{b\bar{j}} = \sum_{\bar{i}P} Y_{\bar{i}P}^{\bar{j}}\Gamma_{bP}^{\bar{i}} - \sum_{aP} Y_{aP}^{b}\Gamma_{aP}^{\bar{j}} - \frac{1}{2}\mathcal{R}\left[\mathbf{D}'\right]_{b\bar{j}} \tag{S21}$$

$$X_{b\underline{j}} = \sum_{\bar{i}P} Y_{\bar{i}P}^{\underline{j}}\Gamma_{bP}^{\bar{i}} - \frac{1}{2}\mathcal{R}\left[\mathbf{D}'\right]_{b\underline{j}} \tag{S22}$$

where

$$D'_{ab} = D''_{ab} \tag{S23}$$

$$D'_{\bar{i}\bar{j}} = D''_{\bar{i}\bar{j}} \tag{S24}$$

$$D'_{\underline{i}\underline{j}} = D''_{\underline{i}\underline{j}} = 0 \tag{S25}$$

$$D'_{\bar{i}\underline{j}} = D'_{\underline{j}\bar{i}} = \frac{1}{2}\check{z}_{\bar{i}\underline{j}} \tag{S26}$$

Analogously, for first order z-vector equations:

$$\begin{aligned} \overline{X}_{b\bar{j}}^{\mathbf{B}} = &\sum_{aP}\left[\Gamma_{aP}^{\bar{j},\mathbf{B}}Y_{aP}^{b} + \Gamma_{aP}^{\bar{j}}Y_{aP}^{b,\mathbf{B}}\right] \\ &- \sum_{\bar{i}P}\left[\Gamma_{bP}^{\bar{i},\mathbf{B}}Y_{\bar{j}P}^{\bar{i}} + \Gamma_{bP}^{\bar{i}}Y_{\bar{j}P}^{\bar{i},\mathbf{B}}\right] \\ &- \frac{1}{2}\sum_{a} z_{a\bar{j}}F_{ab}^{\mathbf{B}} + \frac{1}{2}\sum_{i} z_{bi}F_{\bar{j}i}^{\mathbf{B}} + \sum_{pq} D_{pq}\left(pq\,||\,b\bar{j}\right)^{(\mathbf{B})} \\ &+ \frac{1}{2}\mathcal{R}^{\mathrm{XC}(\mathbf{B})}\left[\mathbf{D}\right]_{b\bar{j}} + \frac{1}{2}\overline{\mathcal{R}}\left[\mathbf{D}'^{\mathbf{B}}\right]_{b\bar{j}} - \frac{1}{2}\sum_{p} U_{pb}^{\mathbf{B}}\mathcal{R}\left[\mathbf{D}\right]_{p\bar{j}} \\ &+ \frac{1}{2}\sum_{p}\mathcal{R}\left[\mathbf{D}\right]_{bp}U_{p\bar{j}}^{\mathbf{B}} - \overline{\mathcal{R}}\left[\mathbf{U}^{\mathbf{B}}\mathbf{D}\right]_{bj} \end{aligned} \tag{S27}$$

$$\begin{aligned} \overline{X}_{b\underline{j}}^{\mathbf{B}} = &-\sum_{\bar{i}P}\left[\Gamma_{bP}^{\bar{i},\mathbf{B}}Y_{\underline{j}P}^{\bar{i}} + \Gamma_{bP}^{\bar{i}}Y_{\underline{j}P}^{\bar{i},\mathbf{B}}\right] \\ &- \frac{1}{2}\sum_{a} z_{a\underline{j}}F_{ab}^{\mathbf{B}} + \frac{1}{2}\sum_{i} z_{bi}F_{\underline{j}i}^{\mathbf{B}} + \sum_{pq} D_{pq}\left(pq\,||\,b\underline{j}\right)^{(\mathbf{B})} \\ &+ \frac{1}{2}\mathcal{R}^{\mathrm{XC}(\mathbf{B})}\left[\mathbf{D}\right]_{b\underline{j}} + \frac{1}{2}\overline{\mathcal{R}}\left[\mathbf{D}'^{\mathbf{B}}\right]_{b\underline{j}} - \frac{1}{2}\sum_{p} U_{pb}^{\mathbf{B}}\mathcal{R}\left[\mathbf{D}\right]_{p\underline{j}} \\ &+ \frac{1}{2}\sum_{p}\mathcal{R}\left[\mathbf{D}\right]_{bp}U_{p\underline{j}}^{\mathbf{B}} - \overline{\mathcal{R}}\left[\mathbf{U}^{\mathbf{B}}\mathbf{D}\right]_{b\underline{j}} \end{aligned} \tag{S28}$$

where

$$D'^{\mathbf{B}}_{ab} = D''^{\mathbf{B}}_{ab} \tag{S29}$$

$$D'^{\mathbf{B}}_{\bar{i}\bar{j}} = D''^{\mathbf{B}}_{\bar{i}\bar{j}} \tag{S30}$$

$$D'^{\mathbf{B}}_{\underline{i}\underline{j}} = D''^{\mathbf{B}}_{\underline{i}\underline{j}} = 0 \tag{S31}$$

$$D'^{\mathbf{B}}_{\bar{i}\underline{k}} = -D'^{\mathbf{B}}_{\underline{k}\bar{i}} = \frac{1}{2}\check{z}^{\mathbf{B}}_{\bar{i}\underline{k}} \tag{S32}$$

$$\begin{aligned} \check{z}^{\mathbf{B}}_{\bar{i}\underline{k}} = &\left(2\sum_{aP}\Gamma_{aP}^{\bar{i},\mathbf{B}}Y_{aP}^{\underline{k}} + 2\sum_{aP}\Gamma_{aP}^{\bar{i}}Y_{aP}^{\underline{k},\mathbf{B}}\right. \\ &\left. - \sum_{\bar{j}}\check{z}_{\bar{j}\underline{k}}F^{\mathbf{B}}_{\bar{j}\bar{i}} + \sum_{\underline{l}}\check{z}_{\bar{i}\underline{l}}F^{\mathbf{B}}_{\underline{k}\underline{l}}\right)\left(\varepsilon_{\bar{i}} - \varepsilon_{\underline{k}}\right)^{-1} \end{aligned} \tag{S33}$$

S4 Implicit Solvation

If an implicit solvation model is used, such as the conductor-like polarizable continuum model (CPCM) implemented in ORCA,[S9] the Fock matrix is corrected with an additional term:

$$F_{\mu\nu} \leftarrow V_{\mu\nu}^{\mathrm{sol}} = v_{\mathrm{nuc}}^{\mathrm{sol}}S_{\mu\nu} + \int v_{\mathbf{P}}^{\mathrm{sol}}\left(\mathbf{r}\right)\Omega_{\mu\nu}\left(\mathbf{r}\right)\mathrm{d}\mathbf{r} \tag{S34}$$

where

$$v_{\mathrm{nuc}}^{\mathrm{sol}}(\mathbf{r}) = -f_\varepsilon \sum_{st} \left(\mathbf{A}^{-1}\right)_{st} |\,\mathbf{r}-\mathbf{r}_s\,|^{-1} \sum_K \frac{Z_K}{|\,\mathbf{R}_K-\mathbf{r}_t\,|} \tag{S35}$$

$$v_{\mathbf{P}}^{\mathrm{sol}}(\mathbf{r}) = f_\varepsilon \sum_{st} \left(\mathbf{A}^{-1}\right)_{st} |\,\mathbf{r}-\mathbf{r}_s\,|^{-1} \int \frac{\rho_{\mathbf{P}}(\mathbf{r}')}{|\,\mathbf{r}'-\mathbf{r}_t\,|}\mathrm{d}\mathbf{r}' \tag{S36}$$

Z_K is the charge of nucleus K and R_K is its position; the indices s and t denote surface tesserae; f_ε is a function, which depends on the dielectric constant of the solvent; and the matrix $\mathbf{A}$ (defined as $\mathbf{S}$ in ref S9) depends on the areas and relative positions of the surface tesserae. Both the nuclear and the electronic terms, $v_{\mathrm{nuc}}^{\mathrm{sol}}$ and $v_{\mathbf{P}}^{\mathrm{sol}}$ respectively, contribute to the CPSCF equations,[S9,S10] but only the latter contributes to the Fock response in the z-vector equations:

$$\mathcal{R}[\mathbf{D}]_{pq} \leftarrow \mathcal{R}^{\mathrm{sol}}[\mathbf{D}]_{pq} = 4\sum_{\mu\nu} c_{\mu p} c_{\nu q} \int v_{\mathbf{D}}^{\mathrm{sol}}(\mathbf{r})\,\Omega_{\mu\nu}(\mathbf{r})\,\mathrm{d}\mathbf{r} \tag{S37}$$

where $v_{\mathbf{D}}^{\mathrm{sol}}$ (for any matrix D) is defined as in eq S36 with $\rho_{\mathbf{D}}$ substituted for $\rho_{\mathbf{P}}$. An additional term enters the first order z-vector equations RHS due to the use of GIAOs:

$$\overline{X}_{aj}^{\mathbf{B}} \leftarrow \frac{1}{2}\mathcal{R}^{\mathrm{sol}(\mathbf{B})}[\mathbf{D}]_{aj} \tag{S38}$$

$$\mathcal{R}^{\mathrm{sol}(\mathbf{B})}[\mathbf{D}]_{pq} = 4\sum_{\mu\nu} c_{\mu p} c_{\nu q} \int v_{\mathbf{D}}^{\mathrm{sol}}(\mathbf{r})\,\Omega_{\mu\nu}^{\mathbf{B}}(\mathbf{r})\,\mathrm{d}\mathbf{r} \tag{S39}$$

S5 Additional Results

Deviations of calculated CSCs and RCSs from empirical equilibrium data are presented in Figures S1 and S2. Scaling of different calculation parts with system size is shown in Figures S3–S5. Contributions to the perturbed MP2 density computation time are presented in Figures S6–S8.

References

(S1) Pople, J. A.; Gill, P. M.; Johnson, B. G. Kohn—Sham density-functional theory within a finite basis set. *Chem. Phys. Lett.* **1992**, *199*, 557–560.

(S2) Neese, F.; Schwabe, T.; Grimme, S. Analytic derivatives for perturbatively corrected "double hybrid" density functionals: Theory, implementation, and applications. *J. Chem. Phys.* **2007**, *126*, 124115.

(S3) Kollwitz, M.; Gauss, J. A direct implementation of the GIAO-MBPT(2) method for calculating NMR chemical shifts. Application to the naphthalenium and anthracenium ions. *Chem. Phys. Lett.* **1996**, *260*, 639–646.

(S4) Lee, T. J.; Rendell, A. P. Analytic gradients for coupled-cluster energies that include noniterative connected triple excitations: Application to cis- and trans-HONO. *J. Chem. Phys.* **1991**, *94*, 6229–6236.

(S5) Lee, T. J.; Racine, S. C.; Rice, J. E.; Rendell, A. P. On the orbital contribution to analytical derivatives of perturbation theory energies. *Mol. Phys.* **1995**, *85*, 561–571.

(S6) Gauss, J.; Stanton, J. F. Perturbative treatment of triple excitations in coupled-cluster calculations of nuclear magnetic shielding constants. *J. Chem. Phys.* **1996**, *104*, 2574–2583.

(S7) Weigend, F.; Häser, M. RI-MP2: first derivatives and global consistency. *Theor. Chem. Accounts Theory, Comput. Model. (Theoretica Chim. Acta)* **1997**, *97*, 331–340.

(S8) Loibl, S.; Schütz, M. NMR shielding tensors for density fitted local second-order Møller-Plesset perturbation theory using gauge including atomic orbitals. *J. Chem. Phys.* **2012**, *137*, 084107.

(S9) Cossi, M.; Rega, N.; Scalmani, G.; Barone, V. Energies, structures, and electronic properties of molecules in solution with the C-PCM solvation model. *J. Comput. Chem.* **2003**, *24*, 669–681.

(S10) Stoychev, G. L.; Auer, A. A.; Izsák, R.; Neese, F. Self-Consistent Field Calculation of Nuclear Magnetic Resonance Chemical Shielding Constants Using Gauge-Including Atomic Orbitals and Approximate Two-Electron Integrals. *J. Chem. Theory Comput.* **2018**, *14*, 619–637.

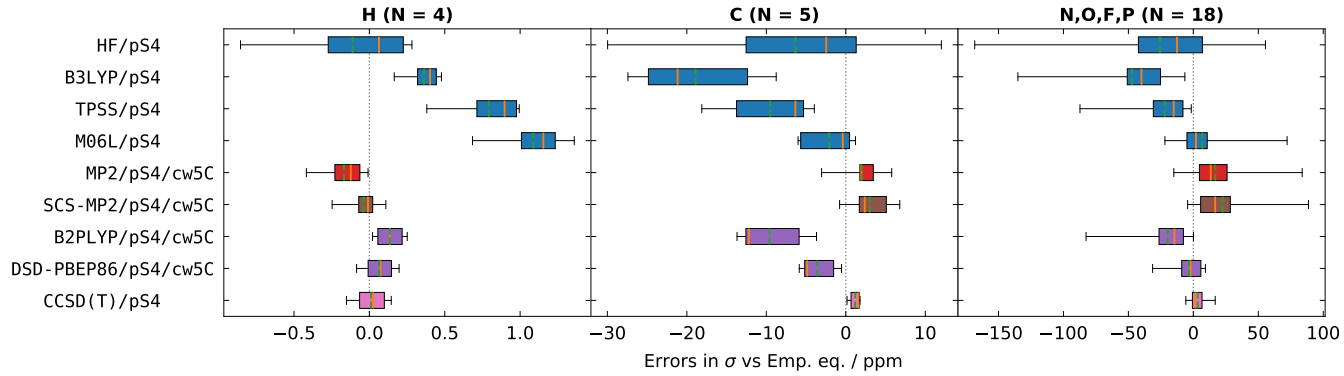

Figure S1: Deviations of chemical shielding constants (ppm) for groups of nuclei, calculated using different methods, from empirical equilibrium values. The number of nuclei in each group is given in parentheses. Boxes show the IQRE_σ, whiskers show the MinE_σ and MaxE_σ, orange lines show the MedE_σ, and green dashed lines show the ME_σ.

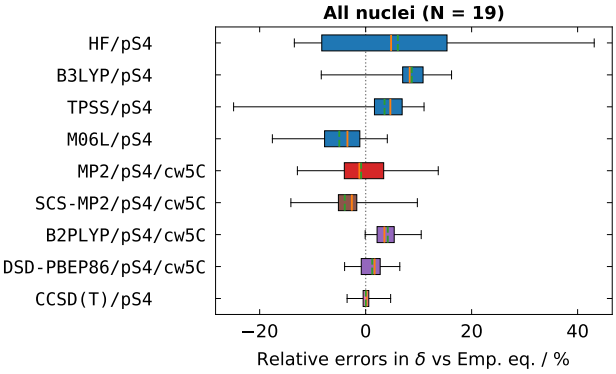

Figure S2: Relative deviations of chemical shifts (%), calculated using different methods, from empirical equilibrium values. The number of data points is given in parentheses. Boxes show the IQRRE_δ, whiskers show the MinRE_δ and MaxRE_δ, orange lines show the MedRE_δ, and green dashed lines show the MRE_δ.

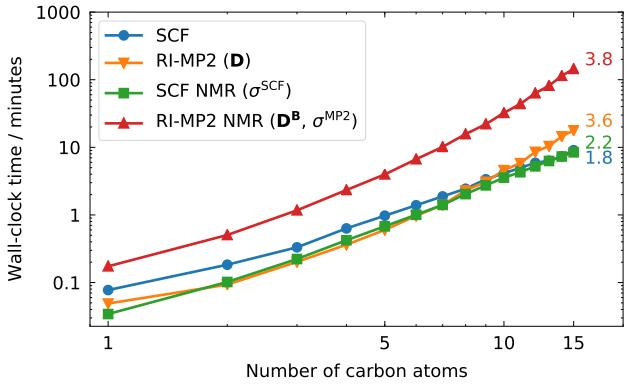

Figure S4: Scaling with system size of different parts of the DSD-PBEP86/pS2/cw3C/RIJCOSX-L computation time for linear alkane chains ($\mathrm{C}_n\mathrm{H}_{(2n+2)}$). The numbers on the right denote the slope of the linear fit (on a log–log scale) of the last five points in each series. The calculations were performed on 8 Intel Xeon E7-8837 2.67 GHz cores with 8 GB RAM per core.

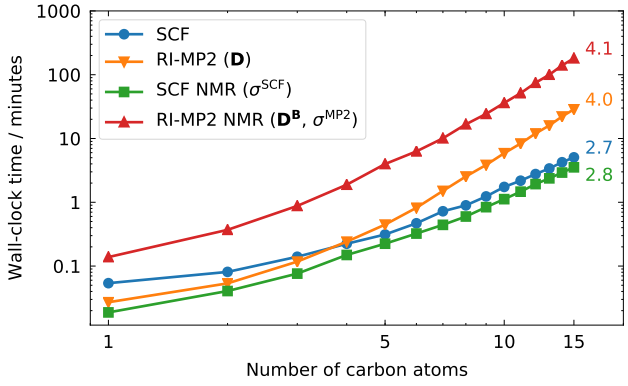

Figure S3: Scaling with system size of different parts of the DSD-PBEP86/pS2/cw3C/RIJK(RITrafo) computation time for linear alkane chains ($\mathrm{C}_n\mathrm{H}_{(2n+2)}$). The numbers on the right denote the slope of the linear fit (on a log–log scale) of the last five points in each series. The calculations were performed on 8 Intel Xeon E7-8837 2.67 GHz cores with 8 GB RAM per core.

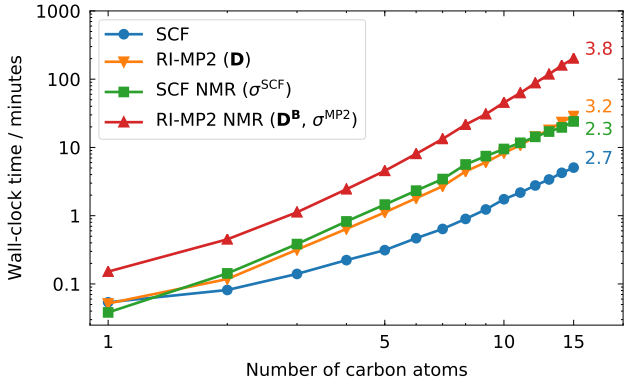

Figure S5: Scaling with system size of different parts of the DSD-PBEP86/pS2/cw3C/RIJK(RIJONX) computation time for linear alkane chains ($\mathrm{C}_n\mathrm{H}_{(2n+2)}$). The numbers on the right denote the slope of the linear fit (on a log–log scale) of the last five points in each series. The calculations were performed on 8 Intel Xeon E7-8837 2.67 GHz cores with 8 GB RAM per core.

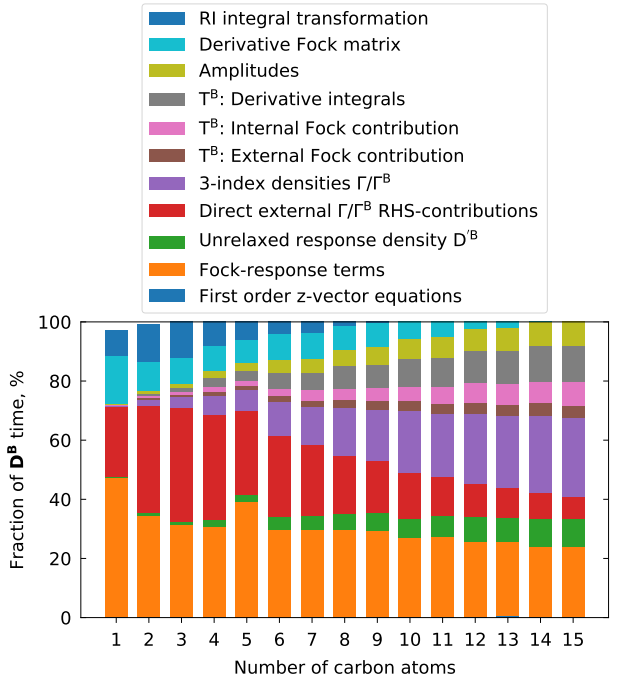

Figure S6: Contributions, adding up to over 97 % of the total $\mathbf{D^B}$ computation time at the DSD-PBEP86/pS2/cw3C/RIJK(RITrafo) level, for linear alkane chains ($C_nH_{(2n+2)}$). The calculations were performed on 8 Intel Xeon E7-8837 2.67 GHz cores with 8 GB RAM per core.

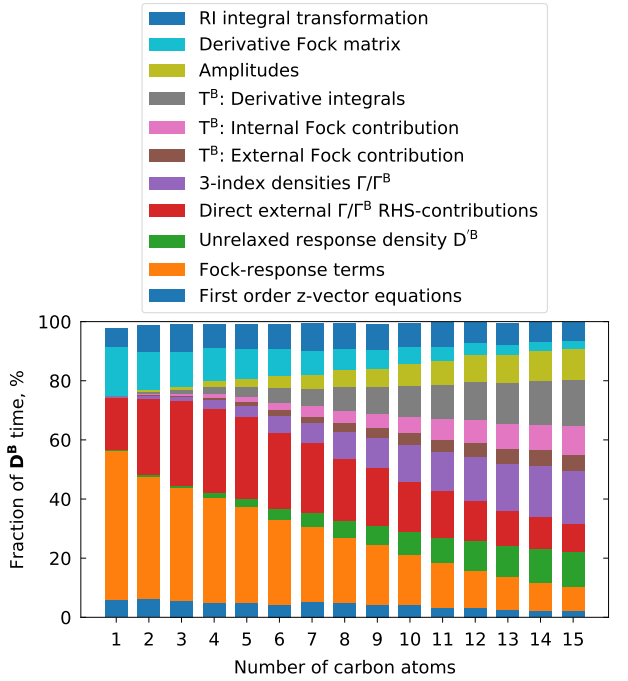

Figure S7: Contributions, adding up to over 97 % of the total $\mathbf{D^B}$ computation time at the DSD-PBEP86/pS2/cw3C/RIJCOSX-L level, for linear alkane chains ($C_nH_{(2n+2)}$). The calculations were performed on 8 Intel Xeon E7-8837 2.67 GHz cores with 8 GB RAM per core.

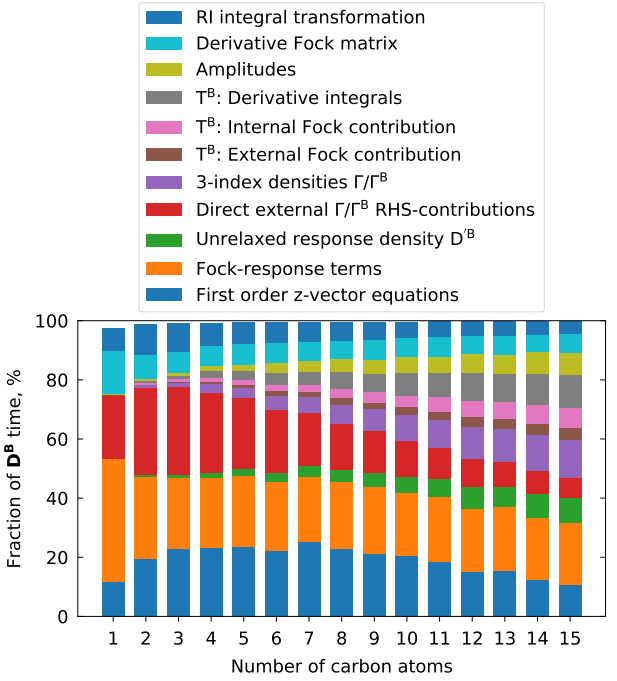

Figure S8: Contributions, adding up to over 97 % of the total $\mathbf{D^B}$ computation time at the DSD-PBEP86/pS2/cw3C/RIJK(RIJONX) level, for linear alkane chains ($C_nH_{(2n+2)}$). The calculations were performed on 8 Intel Xeon E7-8837 2.67 GHz cores with 8 GB RAM per core.